doi:10.2533/chimia.2016.240 Chimia 70 (2016) 240–243

Efficient Water Electrolysis Using Ni_2P as a Bifunctional Catalyst: Unveiling the Oxygen Evolution Catalytic Properties of Ni_2P

Lucas-Alexandre Stern[§] and Xile Hu*

[§]SCS-DSM Award for best poster presentation in Catalysis Science and Engineering

Abstract: The excellent bifunctional catalytic activity of nickel phosphide (Ni_2P) for water splitting is reported. Ni_2P, an active hydrogen evolving catalyst, is shown to be highly active for oxygen evolution. Only 290 mV of overpotential is required to generate a current density of 10 mA cm^{-2} in 1 M KOH. Under oxygen evolving conditions, Ni_2P undergoes structural modification to form a Ni_2P/NiO_x core-shell assembly, the catalytic active species. Ni_2P is applied on both electrodes of an alkaline electrolyser and a current density of 10 mA cm^{-2} is generated at 1.63 V.

Keywords: Electrochemistry · Janus catalyst · Ni_2P · Oxygen evolution · Water splitting

1. Introduction

Global scale exploitation of renewable energy resources, such as wind and solar energy, demands efficient energy storage techniques. Electrochemical water splitting is one of the most attractive method for energy storage.[1] Water splitting is subdivided in two half-reactions, namely, the hydrogen evolution reaction (HER, Eqn. (1)) and the oxygen evolution reaction (OER, Eqn. (2)).

$$2\,H^+ + 2\,e^- \rightarrow H_2 \quad (1)$$

$$2\,H_2O \rightarrow 4\,H^+ + 4\,e^- + O_2 \quad (2)$$

Both reactions require electrocatalysts to proceed efficiently. State-of-the-art catalysts rely on the use of scarce and expensive noble metals, *e.g.* platinum.[2] While promising Earth-abundant water-splitting catalysts have been developed, only few materials are able to catalyse both HER and OER in the same media. Bifunctional catalysts made from Earth-abundant metals would facilitate production and implementation of electrolyser devices. The reported bifunctional systems include Co,[2] Ni,[3] Cu,[4] NiFe LDH,[5] $NiFeO_x$,[6] $NiCo_2S_4$,[7] Ni_5P_4,[8] CoO_x,[9] CoP,[10] FeP.[11] In this article, we show that Ni_2P, an active HER catalyst, is efficient for the oxygen evolution reaction in alkaline medium. Under OER conditions, the material forms a Ni_2P/NiO_x core-shell heterostructure. This assembly generates a current density of 10 mA cm^{-2} at an overpotential of only 290 mV.[12] The Janus behaviour of the material permits the fabrication of an efficient alkaline electrolyser using Ni_2P as catalyst for both the cathode and the anode.

2. Oxygen Evolution Activity of Ni_2P

The Ni_2P nanoparticles were prepared *via* a solid-state thermal reaction previously reported by our group.[13] Briefly, a phosphorus source, NaH_2PO_2 (0.66 g, for analysis, Acros), and a nickel salt, $NiCl_2.6H_2O$ (0.3 g, ReagentPlus®, Aldrich), were ground together at ambient atmosphere and then placed in a quartz boat. This was then transferred into a tubular furnace and heated at 250 °C under a constant flow of nitrogen. The obtained powder was further ground and the impurities were washed off from the product using copious amount of distilled water. The product was then dried in an oven at 50 °C for a few hours. X-ray diffraction of the obtained powder is shown in Fig. 1b. The diffraction signal was compared

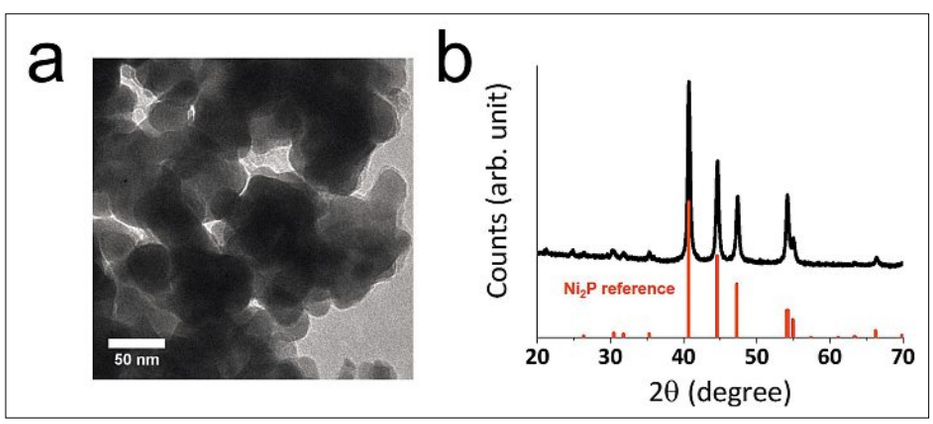

Fig. 1. a) TEM image of polycrystalline Ni_2P. b) Powder X-ray diffraction pattern of the Ni_2P nanoparticles. Adapted by permission of The Royal Society of Chemistry from ref. [12].

*Correspondence: Prof. Dr. X. Hu
Laboratory of Inorganic Synthesis and Catalysis
Institute of Chemical Sciences and Engineering
École Polytechnique Fédérale de Lausanne (EPFL)
ISIC-LSCI, BCH 3305
CH-1015 Lausanne
E-mail: xile.hu@epfl.ch

to the reference diffraction pattern obtained from the International Center of Diffraction Data. The overlapping signals indicated the successful synthesis of pure phase Ni_2P. The transmission electron microscopy (TEM) image shows that the Ni_2P nanoparticles have an averaged size of 50 nm and are coated with a thin amorphous layer (Fig. 1a).

To evaluate the catalytic activity of Ni_2P for the oxygen evolution reaction, linear sweep voltammetry scans were performed in 1 M KOH. The catalytic activity of nickel phosphide was measured and compared to various nanomaterials including IrO_2, Ni, NiO_x and an electrodeposited $Ni(OH)_2$ film (Fig. 2a). IrO_2 (99.9% Ir, abcr) and NiO_x (99.8% trace metals basis, Aldrich) were used as received, while Ni nanoparticles and $Ni(OH)_2$ film preparation has been reported previously.[14] The loading of IrO_2, Ni, NiO_x applied on the glassy carbon electrode was identical to Ni_2P loading. Fig. 2a shows that Ni_2P nanoparticles catalytic activity is superior to that of the different catalysts evaluated. The overpotential to generate a current density of 10 mA cm^{-2} is only 290 mV for Ni_2P. To reach similar current density, IrO_2 and $Ni(OH)_2$ requires an additional 40 mV of overpotential compared to Ni_2P. Ni and NiO_x drive a current density of 10 mA cm^{-2} at 365 mV of overpotential.

The electrochemical surface area (ESCA) of the materials was assessed and compared. For this purpose, the double-layer capacitance of the materials was calculated. Fig. 2b shows the ESCA of the nickel-based catalysts. The ESCA for the different materials were expressed in terms of surface averaged double layer capacitance. Ni_2P have higher surface area for similar loading than other nickel materials: 176.9 µF cm^{-2}, followed by $Ni(OH)_2$ 137.2 µF cm^{-2}. NiO_x and Ni nanoparticles have smaller ESCA values 68 and 37 µF cm^{-2} respectively. The correlation determined between the ESCA of Ni, NiO_x, $Ni(OH)_2$ and their respective catalytic activity at the fixed overpotential of 325 mV cannot be applied to Ni_2P. This indicates that high surface area is not the sole reason for the superior catalytic activity of nickel phosphide.

The stability of the nickel phosphide nanoparticles was probed by galvanostatic experiment. Fig. 2c shows that the overpotential to generate 10 mA cm^{-2} increased only of 10 mV over the course of 10 hours indicating high stability of the catalyst. The nickel phosphide oxygen evolution activity was also compared to several state-of-the-art materials (Table 1). It can be seen that Ni_2P is more active than many Ni and Co-based oxides, and even IrO_2 in base.

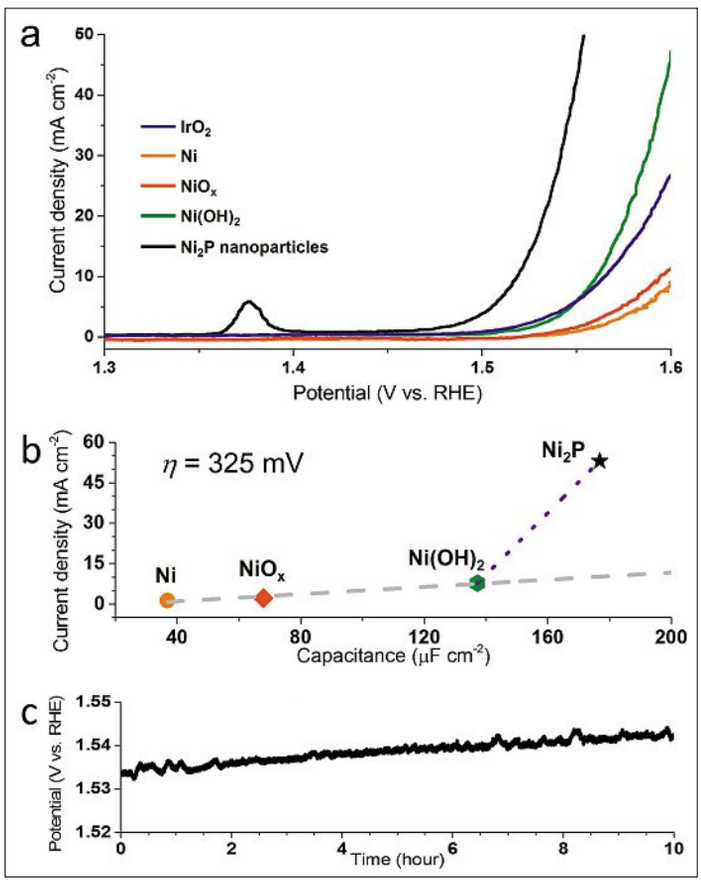

Fig. 2. a) Linear sweep voltammetric (LSV) curves of Ni_2P, Ni nanoparticles, NiO_x nanoparticles, electrodeposited $Ni(OH)_2$, and IrO_2 in 1 M KOH. b) Correlation of the current density at an overpotential of 325 mV, with the electrochemical capacitance of the different nickel materials. c) Galvanostatic measurement on the Ni_2P nanoparticles in 1 M KOH at a constant current density of 10 mA cm^{-2} over 10 h. Conditions: pretreated working electrode, pre-activated Ni_2P catalysts, 5 mV s^{-1}, 0.14 mg cm^{-2}. Adapted by permission of The Royal Society of Chemistry from ref. [12].

Table 1. Comparison of the OER catalytic activity of state-of-the-art catalysts. Adapted by permission of The Royal Society of Chemistry from ref. [12].

Material	Loading [mg cm^{-2}]	η @ 10 mA cm^{-2} [mV]	Ref.
Ni	0.14	377	This work
NiO_x	0.14	364	This work
$Ni(OH)_2$	0.14	331	This work
Ni_2P	0.14	290	This work
NiO_x	0.02	360	[15c]
α-$Ni(OH)_2$	0.20	331	[15d]
β-$Ni(OH)_2$	0.20	444	[15d]
$NiCo_2O_4$	0.53	565	[15e]
NiFe-LDH	0.20	320	[16]
CoO_x@CN	0.42	410	[9]
BSCF82	0.25	320	[17]
IrO_2	-	320	[15b]
IrO_2[a]	0.35	275	[18]

[a]Catalytic activity measured in acidic conditions

3. Ni_2P/NiO_x Core-shell Structure: The OER Catalytic Active Species

To identify the nature of the chemical modifications undergone by nickel phosphide during water oxidation, the Ni_2P nanoparticles were characterized prior and after catalysis by high-resolution TEM, energy-dispersive X-ray element mapping and X-ray photoelectron spectroscopy (XPS) (Fig. 3). The data indicate that prior to catalysis crystalline

nanoparticles of Ni_2P are embedded in an amorphous matrix, which is oxygen-rich, contains phosphorus, and is free of any metallic content (Fig. 3a–e). This layer likely consists of residual P_2O_5 as a side product of the catalyst synthesis. Important structural change can be observed on the catalytic material after oxygen evolution for 1 h. The HRTEM image (Fig. 3g) shows that after OER, the layer surrounding the nanoparticles is composed of ultrafine particles of about 2–3 nm diameter. Closer inspection of the particles in the layer revealed the presence of lattice registry indicative of crystalline materials. Fast Fourier transform (FFT) (Fig. 3g inset) allowed measurement of the crystal lattice spacing of the fine particles. The distance between two crystal planes is characteristic of NiO_x material. A crystal lattice spacing of the material's core was also determined and it is characteristic of the (100) facet of Ni_2P. Elemental mapping images of the catalyst after OER (Fig. 3h–k) clearly show the Ni_2P/NiO_x core-shell heterostructure that the material adopts under oxidative conditions. Nickel is present in both layers of the material. Oxygen coats homogeneously the particle surface. Phosphorus is present only in the core. The structure of the material was further corroborated by XPS measurements (Fig. 3l).[19] Electrochemical measurements also validate the formation of a Ni_2P/NiO_X core-shell heterostructure during OER. The oxidation peak observed is indicative of the Ni^{2+}/Ni^{3+} oxidation in many nickel oxide hydroxide and bimetallic $NiFeO_x$ OER catalysts.[13,15a,15d,20] The pre-activation of the catalyst is, thus, hypothesized to allow the *in situ* formation of a stable Ni_2P/NiO_x core-shell heterostructure with improved OER catalytic properties.

The enhanced catalytic activity of the Ni_2P/NiO_X core-shell structure compared to other NiO_x catalysts for OER has two possible origins. On one hand the unique assembly provides significant improvement in electron conduction.[21] Indeed, the metallic Ni_2P core might provide an efficient electron pathway to the insulating NiO_x shell. On the other hand, Ni_2P allows the *in situ* formation of ultrafine nanoparticles of NiO_x, which allows higher active site exposure. Synergistic effects, which warrant further investigation, may play a role as well.

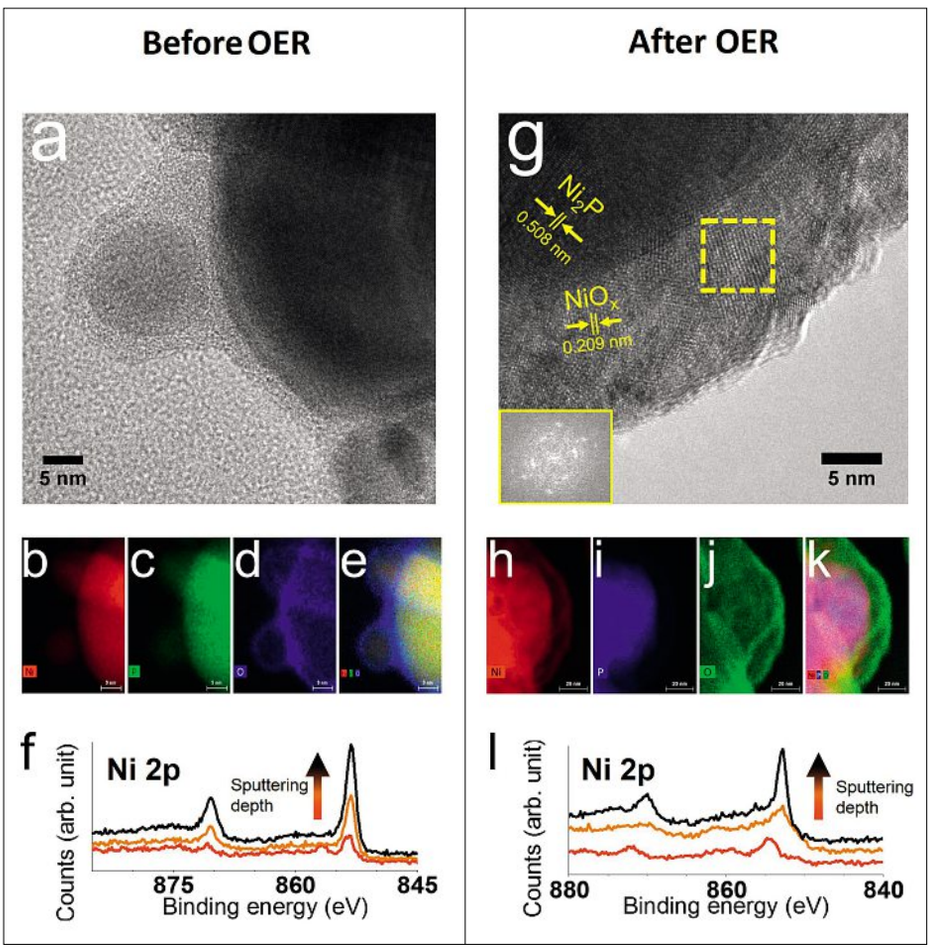

Fig. 3. a) High-resolution TEM (HRTEM) image of the Ni_2P nanoparticles prior to oxygen evolution catalysis. b–e) Corresponding energy dispersive X-ray (EDX) elemental maps of the system prior to catalysis (scale bar: 9 nm). b) Ni elemental mapping. c) Phosphorus elemental mapping. d) Oxygen elemental mapping. e) Combined elemental mapping. f) High-resolution depth-profiling XPS spectra of the Ni 2p area. As the profiling depth increases (arrow direction), the FWHM decreases, indicative of stronger metallic Ni content. g) HRTEM image of the Ni_2P nanoparticles after electrochemical pretreatment at 1.5 V vs. RHE for one hour. Inset (lower left): FFT of the framed area (middle). The spots observed on the FFT are indicative of registry order and so of crystallinity. The lattice fringes spacing of the materials were determined using FFT. They correspond to the characteristic (100) facet of Ni_2P and specific facets of nickel oxides/hydroxides species, NiO_x. h–k) Corresponding EDX maps of the elements on the sample region shown in (g) (scale bar: 20 nm). h) Nickel elemental mapping. i) Phosphorus elemental mapping. j) Oxygen elemental mapping. k) Combined elemental mapping of Ni, O, and P. l) High-resolution depth-profiling XPS spectra of the Ni 2p area after catalytic activity. As the profiling depth increases (arrow direction), the large FWHM, that is indicative of nickel oxide species, decreases, indicative of stronger metallic Ni content. This confirms the presence of a surface oxide layer around metallic nickel phosphide core. Adapted by permission of The Royal Society of Chemistry from ref. [12].

4. Efficient and Inexpensive Alkaline Electrolyser Fabricated Using Ni_2P as Catalyst

The hydrogen evolving capabilities of Ni_2P have been reported recently.[13,22] Given the presented OER catalytic activity, an alkaline electrolyser using Ni_2P as both cathode and anode catalyst was fabricated. The catalyst support used for this device was nickel foam. The loading of catalyst applied on the two Ni foam was 10 mg cm^{-2}. Fig. 4 shows the measured catalytic activity of the alkaline electrolyser in 1 M KOH. The activity is compared with bare Ni foams as reference. To generate a current density of 10 mA cm^{-2} the alkaline electrolyser employing Ni_2P as catalyst only requires 400 mV of overpotential while bare Ni foams demands 560 mV of overpotential to reach the same value of current density.[12] During water electrolysis, the cathode and the anode were separated using a glass frit membrane to avoid any undesirable reactions. The stability of the alkaline electrolyser was tested *via* galvanostatic measurement. A constant current density of 10 mA cm^{-2} was applied for 10 h. Fig. 4 inset shows that the overpotential hardly increases during the course of the experiment and indicates high stability of the fabricated electrolyser. To confirm that all the current generated results from water splitting, the total pressure increase due to hydrogen and oxygen evolution was recorded using a pressure sensor during the electrochemical measurement. The pressure sensor data allows the amount of gas evolved to be calculated over the course of the water electrolysis. The

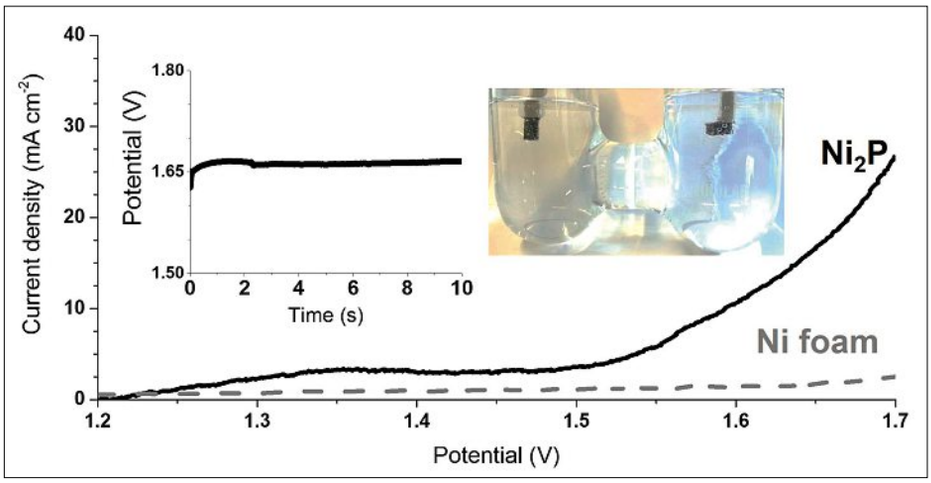

Fig. 4. LSV to evaluate the alkaline electrolyser activity under gas separating conditions. The Ni_2P system (loading 10 mg cm^{-2}, activated anode) necessitates only 400 mV to generate 10 mA cm^{-2}. The Ni foam support was evaluated under similar conditions (gas separation, activated anode but without catalyst) and required 560 mV to generated 10 mA cm^{-2}. A galvanostatic experiment on the Ni_2P alkaline electrolyser with glass frit separation was performed (inset) and indicates the good stability of the system over 10 hours of electrolysis at 10 mA cm^{-2}. An optical photograph illustrates the cell used for these experiments. Adapted by permission of The Royal Society of Chemistry from ref. [12].

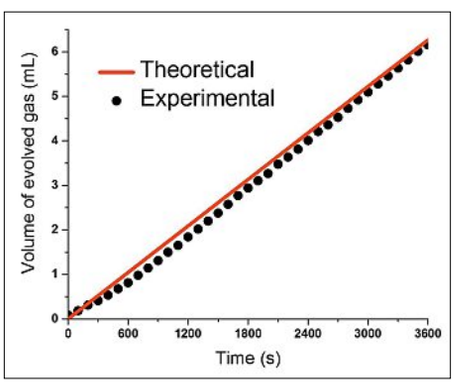

Fig. 5. Faraday yield measurement of the alkaline electrolyser fabricated from Ni_2P loaded Ni foams (loading 10 mg cm^{-2}). The quantity of gas evolved was determined by a pressure sensor. The overlapping lines between the theoretical and experimental values indicate a quantitative Faraday yield of the system, after an induction period of about 250 s. During this induction period, the gas generated are dissolved in the solution to reach an equilibrium. After the induction period, the gas generated can be measured by the pressure sensor. The galvanostatic experiment was performed over 1 h at a constant current density of 10 mA cm^{-2}. The anode was activated prior the galvanostatic experiment. The cathode was used as it is. Adapted by permission of The Royal Society of Chemistry from ref. [12].

theoretical volume of gas evolved can then be calculated by determining the charge passed over the course of the experiment. Comparison between experimental and theoretical volume of gas determines then the Faradaic efficiency of the alkaline electrolyser. Fig. 5 illustrates that the experimental and theoretical amount of gas evolved overlaps indicative of a quantitative Faraday efficiency for the device. Ni_2P is thus an active and stable bifunctional catalyst for water splitting in alkaline media.

5. Conclusion

In summary, Ni_2P is an active catalyst for OER in alkaline conditions. The catalyst is prepared *via* a simple solid-state reaction from abundant and cheap reagents. The catalytic active species is a Ni_2P/NiO_x core-shell heterostructure that is formed *in situ* under OER conditions. The catalytic activity is superior to several state-of-the-art catalysts. The Janus behaviour of the catalyst allows the fabrication of an efficient alkaline electrolyser who generates 10 mA cm^{-2} at an overpotential of only 400 mV. Ni_2P shows promise of potential applications for future devices and highlights the potential of Earth-abundant catalysts as viable electrocatalysts for energy conversion devices and fuel cell applications.

Acknowledgement

This work is supported by the EPFL. We thank Dr. Ligang Feng and Dr. Fang Song at EPFL for assistance in the experiments.

Received: December 1, 2015

[1] N. S. Lewis, D. G. Nocera, *Proc. Natl. Acad. Sci. USA* **2006**, *103*, 15729.
[2] S. Cobo, J. Heidkamp, P.-A. Jacques, J. Fize, V. Fourmond, L. Guetaz, B. Jousselme, V. Ivanova, H. Dau, S. Palacin, M. Fontecave, V. Artero, *Nat. Mater.* **2012**, *11*, 802.
[3] C. He, X. Wu, Z. He, *J. Phys. Chem. C* **2014**, *118*, 4578.
[4] X. Liu, H. Zheng, Z. Sun, A. Han, P. Du, *ACS Catal.* **2015**, *5*, 1530.
[5] J. Luo, J.-H. Im, M. T. Mayer, M. Schreier, M. K. Nazeeruddin, N.-G. Park, S. D. Tilley, H. J. Fan, M. Graetzel, *Science* **2014**, *345*, 1593.
[6] H. Wang, H.-W. Lee, Y. Deng, Z. Lu, P.-C. Hsu, Y. Liu, D. Lin, Y. Cui, *Nat. Commun.* **2015**, *6*, 7261.
[7] D. Liu, Q. Lu, Y. Luo, X. Sun, A. M. Asiri, *Nanoscale* **2015**, *7*, 15122.
[8] M. Ledendecjer, S. K. Calderón, C. Papp, H.-P. Steinrück, M Antonietti, M. Shalom, *Angw. Chem. Int. Ed.* **2015**, *54*, 12361.
[9] H. Jin, J. Wang, D. Su, Z. Wei, Z. Pang, Y. Wang, *J. Am. Chem. Soc.* **2015**, *137*, 2688.
[10] a) N. Jiang, B. You, M. Sheng, Y. Sun, *Angw. Chem. Int. Ed.* **2015**, *54*, 6251; b) Y. Yang, H. Fei, G. Ruan, J. M. Tour, *Adv. Mater.* **2015**, *27*, 3175; c) J. Chang, Y. Xiao, M. Xiao, J. Ge, C. Liu, W. Xing, *ACS Catal.* **2015**, *5*, 6874.
[11] Y. Yan, B. Y. Xia, X. Ge, Z. Liu, A. Fisher, X. Wang, *Chem. Eur. J.* **2015**, *21*, 18062.
[12] L.-A. Stern, L. Feng, F. Song, X. Hu, *Energy Environ. Sci.* **2015**, *8*, 2347.
[13] L. Feng, H. Vrubel, M. Bensimon, X. Hu, *Phys. Chem.Chem. Phys.* **2014**, *16*, 5917.
[14] a) Y. Chen, D.-L. Peng, D. Lin, X. Luo, *nanotechnol.* **2007**, *18*, 505703; b) D. A. Corrigan, R. M. Bendert, *J. Electrochem. Soc.* **1989**, *136*, 723.
[15] a) L. Trotochaud, J. K. Ranney, K. N. Williams, S. W. Boettcher, *J. Am. Chem. Soc.* **2012**, *134*, 17253; b) C. C. L. McCrory, S. H. Jung, J. C. Peters, T. F. Jaramillo, *J. Am. Chem. Soc.* **2013**, *135*, 16977; c) K. Fominykh, J. M. Feckl, J. Sicklinger, M. Doeblinger, S. Boecklein, J. Ziegler, L. Peter, J. Rathousky, E.-W. Scheidt, T. Bein, D. Fattakhova-Rohlfing, *Adv. Funct. Mater.* **2014**, *24*, 3123; d) M. Gao, W. Sheng, Z. Zhuang, Q. Fang, S. Gu, J. Jiang, Y. Yan, *J. Am. Chem. Soc.* **2014**, *136*, 7077; e) H. Shi, G. Zhao, *J. Phys. Chem. C* **2014**, *118*, 25939.
[16] M. Gong, Y. G. Li, H. L. Wang, Y. Y. Liang, J. Z. Wu, J. G. Zhou, J. Wang, T. Regier, F. Wie, H. J. Dai, *J. Am. Chem. Soc.* **2013**, *135*, 8452.
[17] K. J. May, C. E. Carlton, K. A. Stoerzinger, M. Risch, J. Suntivich, Y.-L. Lee, A. Grimaud, Y. Shao-Horn, *J. Phys. Chem. Lett.* **2012**, *3*, 3264.
[18] L. Ouattara, S. Fierro, O. Frey, M. Koudelka, C. Comninellis, *J. Appl. Electrochem.* **2009**, *39*, 1361.
[19] P. E. R. Blanchard, A. P. Grosvenor, R. G. Cavell, A. Mar, *J. Mater. Chem.* **2009**, *19*, 6015.
[20] a) R. L. Doyle, I. J. Godwin, M. P. Brandon, M. E. G. Lyons, *Phys. Chem. Chem. Phys.* **2013**, *15*, 13737; b) L.-A. Stern, X. Hu, *Faraday Discuss.* **2014**, *176*, 363.
[21] a) M. Gong, W. Zhou, M.-C. Tsai, J. Zhou, M. Guan, M.-C. Lin, B. Zhang, Y. Hu, D.-Y. Wang, J. Yang, S. J. Pennycook, B.-J. Hwang, H. Dai, *Nat. Commun.* **2014**, *5*, 4695; b) G. Elmaci, C. E. Frey, P. Kurz, B. Zumreoglu-Karan, *Inorg. Chem.* **2015**, *54*, 2734; c) L. Trotochaud, S. L. Young, J. K. Ranney, S. W. Boettcher, *J. Am. Chem. Soc.* **2014**, *136*, 6744.
[22] E. J. Popczun, J. R. McKone, C. G. Read, A. J. Biacchi, A. M. Wiltrout, N. S. Lewis, R. E. Schaak, *J. Am. Chem. Soc.* **2013**, *135*, 9267.